TAR RNA Recognition by a Cyclic Peptidomimetic of Tat Protein[†,‡]

Thomas C. Leeper,[§] Zafiria Athanassiou,[§] Ricardo L. A. Dias,[||] John A. Robinson,[||] and Gabriele Varani*[,§]

Departments of Biochemistry and Chemistry, University of Washington, Seattle, Washington 98195-1700, and Organic Chemistry Institute, University of Zurich, Winterthurerstrasse 190, 8057 Zurich, Switzerland

Received June 2, 2005; Revised Manuscript Received July 14, 2005

ABSTRACT: The search for new antiviral drugs that repress HIV viral replication by blocking transactivation of viral RNA transcription has long been advocated as an approach to novel antiviral therapy. However, research in this area has so far failed to yield attractive lead compounds because of the insufficient development of RNA-based medicinal chemistry. One difficulty in efforts to inhibit protein−RNA interactions using small druglike molecules is the large surface areas typically found at these interfaces. To overcome this problem, we sought to identify constrained peptidomimetic inhibitors that would provide potential new drug leads. We previously reported the discovery of a cyclic peptide mimic of the RNA-binding domain of BIV Tat protein based on a designed β-hairpin scaffold. We demonstrated that the cyclic peptide bound BIV TAR RNA with an affinity comparable to that of the RNA-binding domain of the Tat protein and inhibited protein binding to the RNA. In this study, we report the structure of the complex of the cyclic peptide bound to BIV TAR RNA determined using heteronuclear NMR methods. The structure reveals a β-hairpin conformation in the bound peptide, which adopts an unexpected orientation in the major groove of the RNA opposite those observed for peptides derived from the Tat protein. This structure suggests many ways in which to optimize the compound and enhance its activity and pharmacological potential and represents a further step in the rational design of a new class of HIV-1 virus replication inhibitors based on peptidomimetic chemistry.

Ribonucleic acid (RNA)/protein[1] complexes play a central role in the life cycle of many RNA viruses and therefore represent attractive targets to develop new antiviral drugs. Inhibitors of key regulatory steps in the viral life cycle functioning by novel mechanisms would also have more favorable characteristics in regards to the emergence of resistance (*1*−*3*). Classical examples of protein−RNA interactions that are essential for viral replication are the Tat proteins and cognate TAR RNAs from the immunodeficiency viruses (*4*). The virally encoded transactivator proteins (Tat) recognize viral RNA regulatory elements (TAR), recruit a kinase [pTEF-B for the human immunodeficiency virus (HIV)] to release the RNA polymerase stalled at the TAR RNA site, increase enzyme processivity, and prevent premature termination of transcription (*5*−*9*). Disruption of the Tat−TAR interaction would prevent viral replication, because the virus depends on this transactivation activity for mRNA production. Considerable structural knowledge has been generated on this important system using both nuclear magnetic resonance (NMR) and X-ray crystallography (*10*−*19*). However, the increase in structural knowledge has not yet led to the development of novel antiviral drugs or even attractive antiviral leads. While many attempts have been made to discover new lead compounds capable of disrupting viral replication by interfering with the Tat−TAR interaction, the specificity and overall activity of the compounds identified have not been sufficient to warrant further pharmacological development.

Among the approaches used in the past with some success, including in some cases the demonstration of some antiviral activity, were peptidomimetic chemistry (*20*−*26*), as well as small molecule drugs derived either from combinatorial or proprietary libraries or from rational structure-based computational searches (*2*, *3*, *15*, *27*−*38*). One reason for the limited activity of inhibitors discovered to date (*27*, *29*) lies in the physical characteristics of the Tat−TAR interface. Protein−RNA interactions form large interfaces, similar in size to those seen in protein−protein complexes. This makes it difficult to disrupt protein−RNA interactions using small molecule inhibitors, as has also been the case for protein−protein complexes. We hypothesized that peptidomimetic chemistry could provide attractive intermediate molecular-weight antagonists of Tat protein function, as demonstrated successfully in programs aimed at discovering new inhibitors of protein−protein interactions (*39*, *40*).

To pursue this strategy, we studied first the Tat−TAR interaction from the bovine immunodeficiency virus (BIV). Similar to other lentiviruses such as HIV, BIV transcriptional activation requires the interaction of the BIV Tat protein with its cognate TAR RNA response element (Figure 1A). This

[†] This work was supported by a grant from NIH−NIAID (to G.V.) and from the SNF (to J.A.R.).

[‡] Coordinates for the BIV-2 peptide/TAR RNA complex have been deposited in the Protein Data Bank (PDB) as entry 2A9X.

* To whom correspondence should be addressed. Telephone: (206) 543-7113. Fax: (206) 685-8665. E-mail: varani@chem.washington.edu.

[§] University of Washington.

[||] University of Zurich.

[1] Abreviations: RNA, ribonucleic acid; HIV, human immunodeficiency virus; BIV, bovine immunodeficiency virus; TAR, transactivation response region; NMR, nuclear magnetic resonance; NOESY, nuclear Overhauser enhancement spectroscopy; HSQC, heteronuclear single-quantum correlation; NOE, nuclear Overhauser effect; RDC, residual dipolar coupling; PDB, Protein Data Bank.

10.1021/bi0510532 CCC: $30.25
Published on Web 08/23/2005

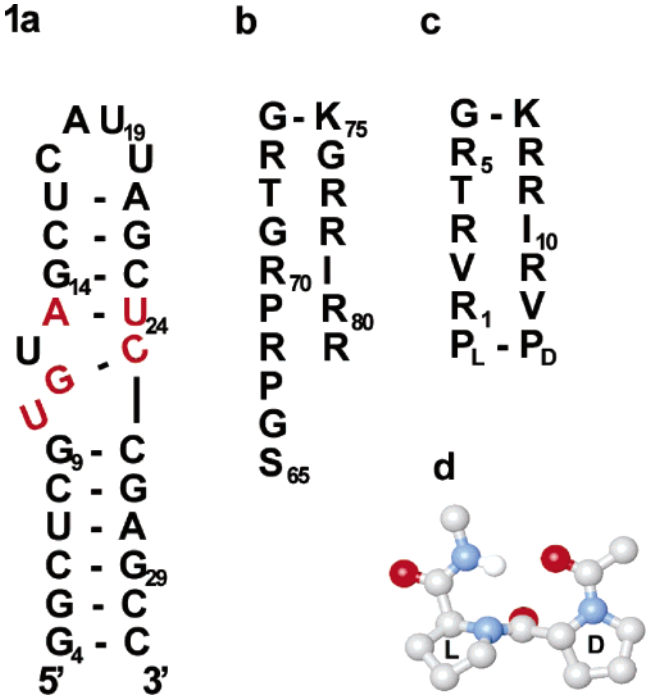

FIGURE 1: (a) BIV TAR RNA construct used in this study, numbered according to the viral RNA; bulge nucleotides that form the base triple and the adjacent G−C pair are highlighted in red. (b) Tat peptide used in the structural studies of the BIV TAT−TAR complex (*17*, *42*). (c) Sequence of the BIV-2 peptidomimetic (*26*). (d) Structure of the D-Pro-L-Pro motif present in BIV-2 is shown to highlight the orientation of the C_α atoms that nucleate β-hairpin formation.

system has been studied extensively (*41*), and structures of the complex between the RNA-binding domain of BIV Tat (Figure 1B) and the cognate TAR RNA are available (*17*, *42*). Thus, unlike the HIV system where the structure of the Tat−TAR complex is still missing, information was available to guide peptidomimetic design. Because BIV is the closest relative to HIV among all lentiviruses, we reasoned that discovery of specific inhibitors of the BIV Tat−TAR interaction would provide useful insights into inhibition of HIV Tat−TAR. Indeed, this hypothesis has been validated by our discovery of potent and specific inhibitors of the HIV Tat−TAR interaction among peptides closely related to the family of peptidometics characterized in the present study (Athanassou et al., data not shown).

We recently demonstrated that a mimic of the BIV Tat protein could be obtained from a small library of conformationally restrained cyclic peptides (*26*). Inclusion of a D-Pro-L-Pro template (Figure 1D) pre-organized this peptide into a β-hairpin conformation in aqueous solution: restraining the peptide in a β-hairpin conformation strongly favored binding. On the basis of the hypothesis that certain residue contacts might be conserved between the wild-type peptide sequence and successful library hits, we retained several arginines within the library sequences, as well as an isoleucine present within the middle region of the BIV Tat protein. However, we added hydrophobic residues near the D-Pro-L-Pro template to stabilize the β-hairpin conformation (*26*). The best cyclic peptide library member, BIV-2 (Figure 1C), binds to BIV TAR RNA with an affinity (K_d = 150 nM) comparable to that observed for the RNA-binding domain from the complete protein (K_d = 50 nM). We report here the structure of the complex between the BIV-2 peptidomimetic and BIV TAR RNA, which reveals an unexpected mode of binding of the mimetic in the major groove of the RNA. Isotopically labeled RNA and refinement with residual dipolar coupling (RDC) allowed a structure of very high quality that will guide further synthetic elaboration of this peptidomimetic.

MATERIALS AND METHODS

RNA Synthesis. BIV TAR RNA samples were made as described previously (*26*, *43*). Briefly, RNA was transcribed *in vitro* from DNA oligonucleotide templates with T7 RNA polymerase purified *in house*. For producing labeled RNA, $^{13}C/^{15}N$-enriched NTPs (Silantes) were substituted for unlabeled NTPs. RNA was purified from crude transcriptions (6 mL) by denaturing polyacrylamide gel electrophoresis (PAGE), electroelution, and concentration by ethanol precipitation. After extensive dialysis into 20 mM sodium acetate (pH 5.5), the RNA was diluted 10-fold, annealed at a dilute concentration by heating briefly to 80 °C and concentrated by lyophilization. The final RNA concentration was determined by UV spectrophotometry at 260 nM. NMR samples for the complex were at concentrations between 600 and 800 μM, except for RDC measurements, where the samples were at 250 μM. For experiments studying nonexchangeable protons, samples were exchanged into D_2O via three cycles of dissolution with 99.99% D_2O and lyophilization. Samples used to study exchangeable protons were dissolved in buffered 92% H_2O/8% D_2O. Dry peptide was added to predialyzed TAR RNA in NMR buffer to achieve complex formation. Formation of a 1:1 complex was established by adding RNA and/or peptide in small increments and monitoring the H5/H6 region of TOCSY spectra of the RNA for the expected number of pyrimidine resonances until one single species was observed corresponding to peptide-bound RNA.

Peptide Synthesis. The BIV-2 peptide was synthesized by solid-phase synthesis and purified by reverse-phase HPLC, as described previously (*26*).

NMR Spectroscopy. NMR data were collected on Bruker DRX 500 MHz, DMX 600 MHz, and DMX 750 MHz spectrometers equipped with HCN and HCP probes with triple-axis gradients. Data were processed with nmrPipe (*44*) and visualized with Sparky (*45*). For 2D ^1H nuclear Overhauser enhancement spectroscopy (NOESY) spectra at 750 MHz, three mixing times (80, 120, and 300 ms) were used; for 3D ^{13}C NOESY−HMQC spectra recorded at 600 MHz, mixing times of 100 and 200 ms were used. ^{13}C frequency spectral widths were set to 24 ppm, and ribose resonances were folded into convenient spectral regions. HCP and HETCOR spectra at 500 MHz were implemented using standard parameters (*46*, *47*) to assign phosphorus atoms and for the determination of backbone torsion angles (see below). Filtered spectra of the "F1fF2f" type were obtained according to published pulse programs (*48*, *49*), except that single purge elements were used to enhance sensitivity. The 2D F1fF2f NOESY spectrum on the bound unlabeled peptide had mixing times of 100 ms, and the F1fF2f TOCSY spectrum employed a 40 ms DIPSY-2 spin lock period (*50*).

Spectral Assignments. Resonance assignments were based on standard NMR methods (*51*). Briefly, NOESY spectra

collected on unlabeled samples at 750 MHz were analyzed to generate initial proton assignments. Adenine H2 protons were clearly identified in spectra collected on samples in water and allowed confident assignment of exchangeable protons (*51*). HCCH−COSY (*52*) and 3D ^{13}C-NOESY−HMQC experiments were used to complete the proton assignments and to assign the carbon resonances. ^{15}N chemical shifts were obtained from ^{15}N-heteronuclear single-quantum correlation (HSQC) and NOESY experiments recorded in water. For the most part, only chemical shifts for RNA residues C8−U16, U19, U20, and G22−G27 and the core peptide-binding region were significantly shifted upon peptide binding. This is consistent with the structure, where the peptide makes very limited contacts above residues U16 and G22 and no contacts at all below residues C8 and G27.

The assignment of the peptide resonances in the complex was greatly aided by filtered/edited NOESY experiments (*48*). Because many of the peptide aliphatic protons resonate in the same region of the NOESY spectrum as ribose resonances, these spectra allowed the discrimination of intraresidue nuclear Overhauser effects (NOEs) in peptide aliphatics from intermolecular NOEs. The typical β-sheet H_α to HN (i to $i + 1$) NOEs facilitated the sequential assignment of the peptide without heteronuclear labeling. Unambiguous observation of $H_\alpha-H_\alpha$ NOEs would not have been possible without the use of the filtered experiments mentioned above.

Residual Dipolar Couplings (RDCs). The RNA/peptide complex used for RDC measurements (225 μL) was mixed with 83 μL of 56 mg/mL Pf1 phage (*53*) purchased from ASLA Ltd. (Riga, Latvia) dialyzed against 20 mM sodium acetate at pH 5.5. The deuterium splitting of this sample was determined to be 12.5 Hz at 300 MHz with no center peak, indicating homogeneous orientation. RDCs were obtained from In-Phase-Anti-Phase (IPAP) HSQC spectra (*54*) collected at 500 Mz and 25 °C. RDCs were measured in the direct (^{1}H) dimension to take advantage of the enhanced digital resolution. The large carbon spectral widths and differing ^{13}C-^{13}C coupling constants required measuring aromatic and ribose RDCs in separate spectra. Reference couplings were determined in the absence of phage, and the following equation was used, $\mathrm{RDC} = J_{\mathrm{w/pf1}} - J_{\mathrm{w/outpf1}}$, where $J_{\mathrm{w/pf1}}$ is the apparent heteronuclear one-bond ^{1}H/^{13}C coupling measured in the presence of phages and $J_{\mathrm{w/outpf1}}$ is the one-bond ^{1}H/^{13}C coupling measure in the absence of phages.

Structure Determination. Structures of the BIV-2/BIV RNA complex were calculated with the Xplor-NIH software package using torsion angle dynamics and simulated annealing (*55*) from a single extended starting template. A total of 100 structures were calculated without RDCs to check for convergence. At this stage of refinement, there were no NOE violations greater than 0.5 Å or dihedral violations greater than 5° for >50 of the calculated structures. RDCs obtained from well-ordered residues, 4−11, 13−18, and 20−31, were used only at this stage of the refinement.

Distance restraints were derived from NOE intensities at 80 and 120 ms mixing times in 2D NOESY spectra recorded at 750 MHz. Restraints for overlapped regions were obtained from the 3D ^{13}C-NOESY−HSQC spectrum recorded at 120 ms mixing time acquired at 600 MHz. Intramolecular peptide distances were obtained from ^{12}C-filtered experiments in 100% D_2O or 90% H_2O. Base-pair planarity and standard hydrogen-bonding restraints were used for unambiguously established base pairs. The U10 to A13/U24 base triple was at first not constrained by hydrogen-bond restraints, but consistent positioning of the base of U10 poised to hydrogen bond to the N7 of A13 verified the hydrogen-bonding pattern for this interaction. Furthermore, the U10 NH has a very clear close NOE contact to A13 H8; in subsequent refinement stages, the base triple was further restrained via hydrogen-bonding constraints.

Backbone and ribose dihedral angle restraints were determined by qualitative analysis of through-bond experiments (2D TOCSY, 2D COSY, and 3D ^{13}C TOCSY−HSQC) (*51*). The glycosidic angle of A18 was restrained to the syn conformation (0 ± 90°) based on the presence of a strong H1′ to H8 NOE. Sugar puckers were constrained to C3′-endo ($\eta0 = 6$, $\eta1 = -25°$, $\eta2 = 37°$, $\eta3 = -33°$, and $\eta4 = 17°$; ±15° for each) for all riboses without appreciable H1′−H2′ cross-peaks in DQF−COSY and 3D ^{13}C-separated TOCSY spectra. Residues with C2′-endo pucker ($\eta0 = -22°$, $\eta1 = 35 \pm 10°$, $\eta2 = -35°$, $\eta3 = 22°$, and $\eta4 = 0°$; ±15°) were U12, U20, A21, and G22, as determined by strong H1′−H2′ correlations in both spectra. The remaining backbone torsion angles were restrained using established methods (*51*). Briefly, dihedral angles α and ζ were set to exclude the trans torsion angle for residues with canonical ^{31}P chemical-shift values; β was restrained to trans; and γ was restrained to g^+ for residues with strong $^4J_{H4'}$/P correlations in the ^{1}H/^{31}P HETCOR spectra. The angle ϵ was restrained to trans when an H2′ to P($i + 1$) peak was observed in either HCP or HETCOR spectra.

RDCs for well-defined residues (G4−G9, G11, A13−U16, and 21−31) were applied as susceptibility anisotropy (*sani*) restraints with a harmonic potential well, eliminating the need to determine error values for each RDC individually. The powder pattern-like distribution of RDCs (*56*) for the BIV TAR RNA in the presence of the cyclic BIV-2 peptide indicated values for the magnitude (D_a) and rhombicity (R) close to −16 and 0.6, respectively. The RDC values were then plotted as a function of topological arrangement (*57*), which revealed a uniform spread in the RDCs over the full RNA. This observation indicated that the TAR RNA in the presence of BIV-2 is significantly more rigid than the free RNA and permitted the use of a single D_a and R to refine the structure. Optimal values of D_a and R were then determined by a systematic grid search sampling values of D_a between −12 and −30 in 1 Hz increments and values of R ranging from 0.2 to 0.6 in 0.05 increments, as described previously (*58*). The set of structures calculated with $D_a = -19$ and $R = 0.3$ had the lowest *sani* energy, and thus, those values were used during the final refinement. Structures of the BIV-2 complex were examined in MolMol (*59*).

RESULTS

Spectral Analysis and Assignments. The structure of the complex between the BIV-2 cyclic peptide and BIV TAR RNA was determined by NMR spectroscopy. Heteronuclear ^{13}C/^{15}N labeling of TAR RNA allowed nearly complete assignments (Figure 2) and good resolution even for the crowded ribose region, using standard methods (*51*). The pattern of $i-i + 1$ H_α to NH NOESY cross-peaks charac-

a

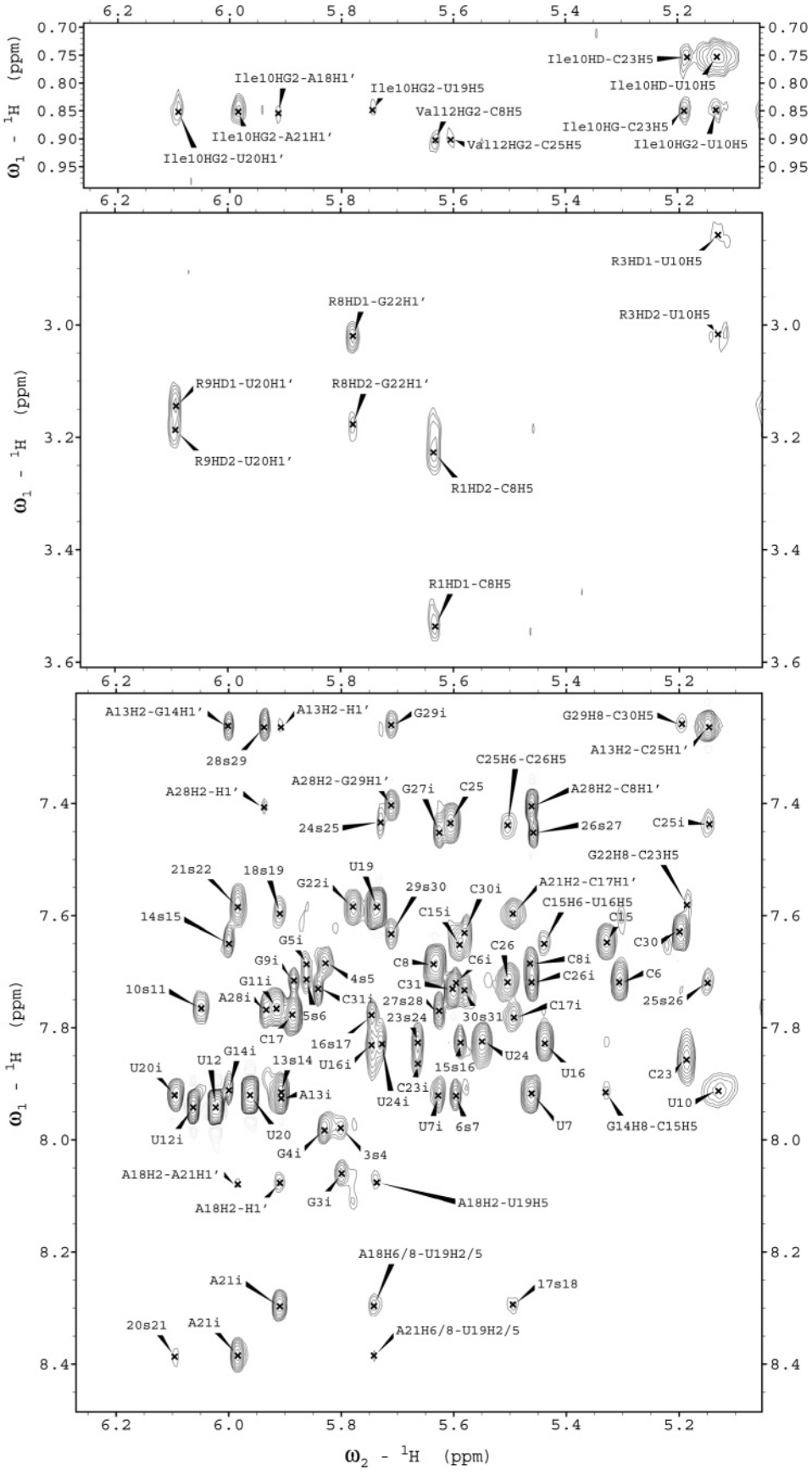
Ile10HD-C23H5
Ile10HD-U10H5
Ile10HG2-A18H1'
Ile10HG2-U19H5
Val12HG2-C8H5
Ile10HG-C23H5
Ile10HG2-A21H1'
Val12HG2-C25H5
Ile10HG2-U10H5
Ile10HG2-U20H1'
R3HD1-U10H5
R8HD1-G22H1'
R3HD2-U10H5
R9HD1-U20H1'
R8HD2-G22H1'
R9HD2-U20H1'
R1HD2-C8H5
R1HD1-C8H5
A13H2-G14H1'
A13H2-H1'
G29i
G29H8-C30H5
A13H2-C25H1'
28s29
C25H6-C26H5
A28H2-G29H1'
G27i
C25
A28H2-C8H1'
A28H2-H1'
24s25
26s27
C25i
G22H8-C23H5
21s22
18s19
U19
A21H2-C17H1'
G22i
29s30
C30i
C15H6-U16H5
14s15
C15i
C15
C30
G5i
C26
C8
C6i
C8i
G9i
C26i
C6
G11i
4s5
C31
10s11
A28i
C31i
27s28
C17i
25s26
5s6
23s24
30s31
C17
16s17
U24
U16
U20i
U12
G14i
13s14
U16i
15s16
C23
C23i
A13i
U24i
U10
U7i
6s7
U7
G14H8-C15H5
U12i
U20
G4i
3s4
A18H2-A21H1'
A18H2-H1'
G3i
A18H2-U19H5
A18H6/8-U19H2/5
A21i
17s18
20s21
A21i
A21H6/8-U19H2/5
ω_1 - ^{1}H (ppm)
ω_2 - ^{1}H (ppm)

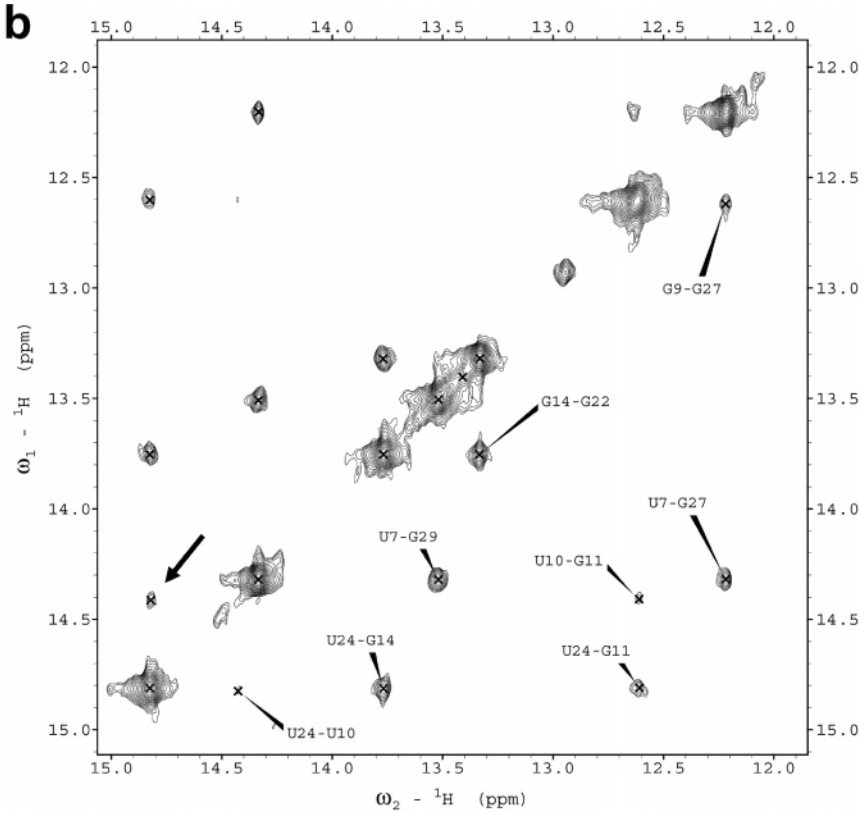

FIGURE 2: (a) Regions of the 300 ms mixing-time NOESY spectrum of the BIV-2 complex with BIV TAR RNA. The three panels show NOEs between the peptide methyl (top), argininine methylene (middle), and RNA aromatic (bottom) to RNA anomeric resonances. (b) The imino−imino region of the 200 ms mixing-time NOESY collected in H_2O highlights the network of connectivities defining the base triple. Of particular interest is the "extra" imino−imino NOE, highlighted by a black arrow, between U24 H3 and U10 H3.

teristic of an antiparallel β hairpin was used for the sequential assignment of the peptide. Assignments of the BIV-2 peptide were nonetheless greatly aided by recording ^{13}C-filtered experiments (*48*) on the complex to distinguish intra- from intermolecular NOE interactions. Three types of filtered experiments were collected: ^{12}C $\omega_1\omega_2$-filtered NOESY in 90% H_2O/10% D_2O, ^{12}C $\omega_1\omega_2$-filtered NOESY in 100% D_2O, and ^{12}C $\omega_1\omega_2$-filtered TOCSY in H_2O/10% D_2O. The filtered NOESY spectrum recorded in water helped distinguish peptide NH−NH and NH to aliphatic NOEs from peptide NH to RNA amino or ribose NOEs. NOESY data recorded in D_2O allowed the unambiguous identification of intramolecular NOEs involving peptide aliphatic resonances, by distinguishing them from NOEs to RNA ribose protons. Side-chain resonances were assigned using the ^{12}C-filtered TOCSY and ^{12}C-filtered NOESY spectra to link side-chain resonances to the backbone assignments. Because of the β-hairpin conformation, many side chains had a clear pattern of side-chain NOEs involving residues i and $i + 2$ within each face of the β sheet.

A number of NMR spectral properties are consistent with BIV TAR RNA, forming a structure very similar to that reported for its complex with BIV Tat protein (*17*, *42*). The U10 NH is involved in a base triple and has a readily observable NOE to A13's H8; the line widths for base H6 and H5 protons of U12 are very sharp, consistent with the base bulging upon complex formation (Figure 2). Furthermore, a continuous network of base NH−NH NOEs extending through the bulge showed the pattern characteristic of the base triple, with the U24 NH having unusual NOEs to three other imino resonances (Figure 2b). The H3′ proton of G11 is significantly downfield-shifted because of the presence of the neighboring U10 (see the Supporting Information). Additionally, the proton assignments of the TAR/BIV-2 terminal loop (C17−U20) were very similar to those reported for the BIV peptide complex with BIV TAR (see the Supporting Information). When these results are taken together, they strongly suggest that the conformation of bound TAR RNA in the presence of the BIV2 peptidomimetic is very similar to that observed for TAR bound to a minimal RNA-binding peptide from the BIV Tat protein (*17*, *42*).

Structure Determination. Intermolecular NOEs between the BIV-2 peptide and TAR RNA were readily observable in 2D (Figure 2) and 3D NOESY spectra. A total of 107 intermolecular NOEs, including 15 NOEs to Arg Hϵ's, were obtained. This number is considerably more than found in one previous study (*17*) and slightly more than the 102 intermolecular NOEs used in a second study (*42*) of the structure of the BIV Tat−TAR complex. However, Arg guanidinium NH_2's were not observable in our spectra, unlike those in other studies (*17*, *42*). This may be due to the slightly weaker affinity of the BIV-2 complex relative to the wild-type complex, to small variations in the solution conditions between the two studies (e.g., pH), or to different kinetic properties of the two complexes. Furthermore, the chemical synthesis of the cyclic peptide precluded economic incorporation of ^{13}C or ^{15}N labels, so that through-bond couplings via hydrogen bonds to exchange-broadened protons could not be obtained.

RDCs for the ^{13}C-labeled RNA in the complex obtained by partial alignment of the complex in pf1 phage (*53*) and

Table 1: Structural Statistics

total number of restraints	829
NOE-derived restraints	533
intermolecular NOEs	107
RNA (intramolecular)	348
peptide (intramolecular)	78
dihedral restraints	165
dipolar coupling restraints	55
hydrogen-bonding restraints	64
planarity restraints	12
average rmsd values from experimental restraints	
distance (Å)	0.05
dihedral (deg)	1.31
RDC (Hz)	2.41
average rmsd values from ideal geometries	
bonds (Å)	0.004
angles (deg)	0.82
improper (deg)	0.46
heavy atom rmsd from mean structure (Å)	
BIV-2 (all backbone atoms)	0.48
TAR RNA (all heavy atoms)	1.07
TAR RNA core, C6−G11, A13−U16, A21−G29[a]	0.66
BIV-2 peptide core, 1, 3, 5, 8, 9, 10, 12[b]	1.15
BIV-2 and TAR core ($a + b$)	0.79
entire structure	1.15

IPAP−HSQC (*54*) were critical to obtain a high-quality structure. The 55 ^{13}C RDCs that were measured accurately significantly improved the global precision of the RNA structure from ∼2 Å (all heavy atoms) to ∼1 Å when RDCs were included (Table 1). The structural accuracy was only minimally improved by RDCs, because the structures of the core bulge region (G9−G11, A13, and U24−C26) with and without RDC refinement are within 0.5 Å of each other (data not shown). Thus, the average structures calculated with and without RDCs were very similar (i.e., no change in accuracy), but the variance in the envelope of their respective ensembles was significantly improved by RDC addition (i.e., improved precision).

The structure of the complex was calculated with Xplor-NIH (*55*) based on a significant number of restraints per residue (Table 1) that compare favorably with those used for studies of the BIV Tat−TAR complex (*17*, *42*). Of the 100 structures calculated, 23 had no NOE violation greater than 0.5 Å or dihedral violations greater than 5°. On average, these structures only had 4 NOE violations greater than 0.2 Å. Of the 23 structures thus deemed to have converged, the 10 lowest energy structures were selected for presentation as the final ensemble. These top 10 structures superimpose very well (Table 1 and Figure 3) with core residues converging to within 0.8 Å root-mean-square deviation (rmsd) (Figure 4A). The previous NMR structures of the Tat−TAR complex had rmsd values over similar regions of 1.16 Å (*42*) and 1.49 Å (*17*), respectively.

Structure of the BIV-2 Peptidomimetic BIV TAR Complex. The core structure of this complex (RNA residues 6−11, 13−16, and 21−29 and peptide residues 1, 3, 5, 8, 9, 10, and 12; Figure 4A) is similar to the structure from which the peptide was designed to mimic the Tat protein but with one very significant difference. The RNA structures only differ by about 1.7 Å over RNA residues 10−13 and 23−25, i.e., the base triple region (Figure 4B). However, the D-Pro-L-Pro template is positioned toward the bottom of the binding region (parts A and C of Figure 4), and the type-II β turn formed by Gly6 and Lys7 points instead away from the 5′ and 3′ ends of the RNA and toward the apical loop.

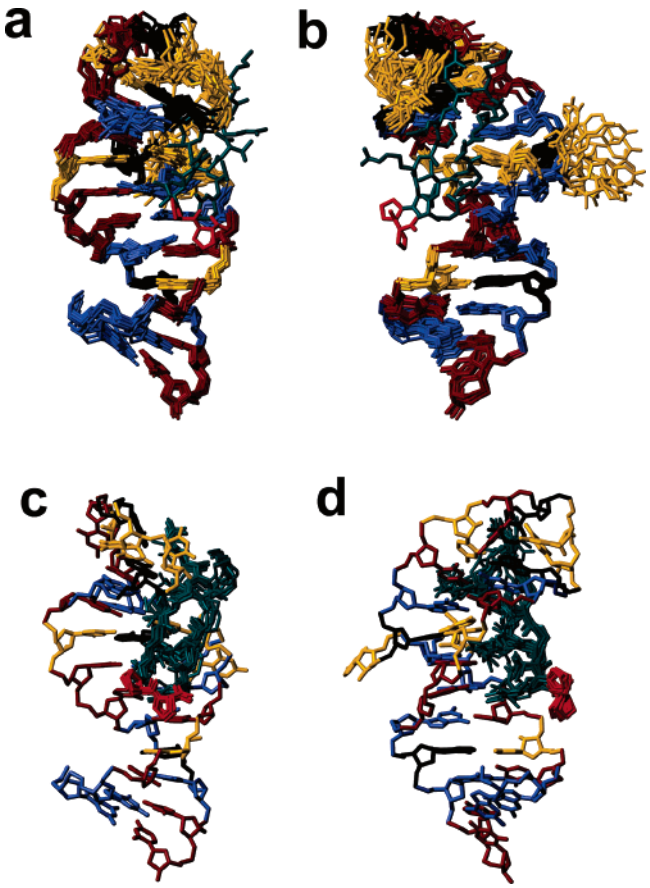

FIGURE 3: Superposition of the 10 structures representing the ensemble of converged structures of the BIV-2 TAR complex. All heavy atoms are shown. Adenines are rendered in black; guanines are rendered in blue; uracyls are rendered in gold; cytosines are rendered in dark red; and the BIV-2 peptide is rendered in bluish green and red (D-Pro-L-Pro template). (a and b) All RNA heavy atoms from the 10 structures are shown with a single view of the peptide derived from the lowest energy structure. (c and d) All 10 peptide structures are shown with the RNA from the lowest energy structure; peptide side chains are only shown for the structurally well-defined residues of the RNA-binding interface and the proline template. The two sets of panels differ by a 90° rotation to highlight the deep penetration of the peptide into the major groove.

This orientation is opposite to what is observed in the Tat protein (Figure 4C), because the D-Pro-L-Pro template was introduced to bridge the gap between the N and C termini of the BIV peptide, and we predicted this orientation would be found where Gly6 and Lys7 lie instead (*26*). Thus, the BIV-2 peptide binds upside down relative to the orientation observed for the wild-type protein. This inversion pivots around the side chain of Ile10 (corresponding to Ile79 in the Tat-derived peptide) that maintains the contacts to the base triple (Figure 5) that is key to the stabilization of the new TAR conformation observed in the protein complex (*17*, *42*). We took great care to verify that the peptide orientation is correct, and several pieces of data provide unambiguous verification of these results. The Val12 methyl protons have very clear NOEs to the H5 and H6 protons of C8 and U9 in the lower stem; the Hγ and Hβ of Arg8 and Arg9 both have clear NOEs to the ribose protons of U16; and Arg9 Hδ and Hϵ have NOEs to the H2 proton of A18.

Intermolecular Interactions and Specificity of the Interaction. The contacts between Ile10 and the bulged U10 of the base triple are conserved between the complexes of TAR

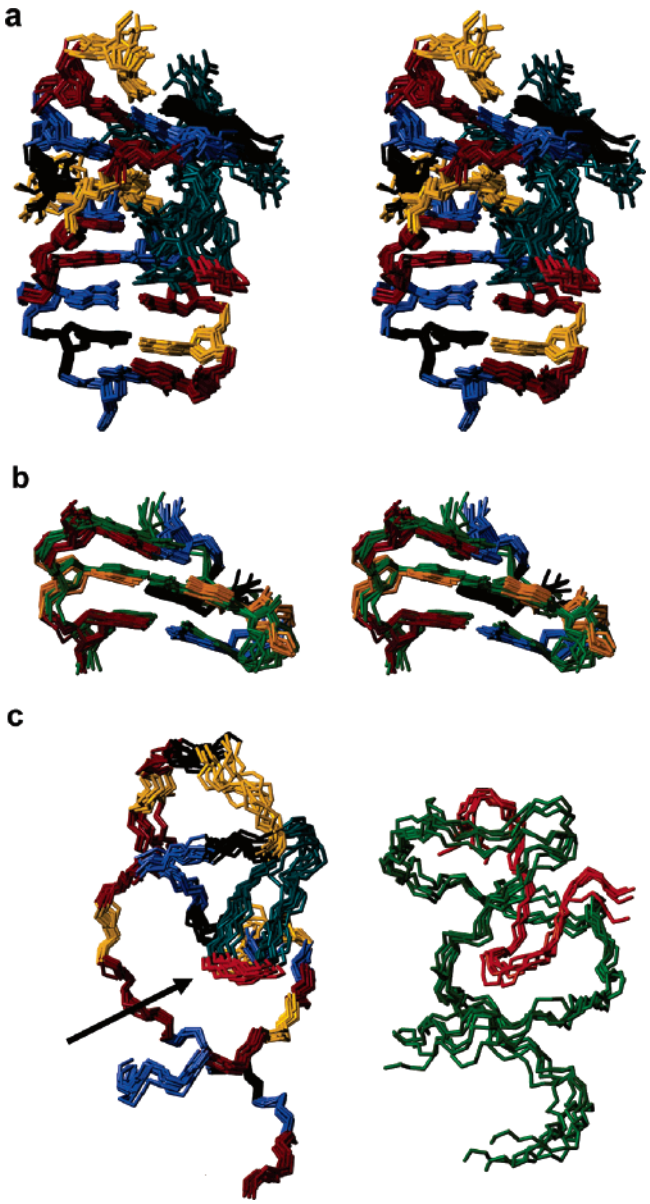

FIGURE 4: (a) Stereoview of the full ensemble (all heavy atoms for all 10 RNA and peptide structures) of the core peptide/RNA interaction region (see Table 1). (b) Superposition of the base triple region (RNA residues 9−11, 13, and 24−26) of the ensemble of BIV-2/TAR structures (black, blue, gold, and red) and for the ensemble of structures of the BIV Tat−TAR complex (green) (*42*), showing the very similar RNA conformations. (c) Backbone traces are shown for the BIV-2/TAR complex (left) and for the BIV Tat−TAR complex (right, orange and bright green) (*42*), indicating the opposite orientation of the two peptides relative to the RNA (see the text). The D-Pro-L-Pro is shown in red and highlighted with an arrow.

RNA with this cyclic peptide mimetic and with the Tat protein (Figure 5A). Thus, the burial of the hydrophobic Ile10 side chain is probably the major driving force to induce the conformational change in TAR and to direct binding. This is the only contact that is strictly conserved between the two structures. The other contacts described below are similar to interactions observed for the Tat peptide, but because of the peptide orientation, there is no direct correspondence. For example, we observe two arginines on the same strand (Arg1 and Arg3) to interact with G9 and G11 (see below), while in the Tat peptide, it is two arginines across from one another on one face of the hairpin that interact with the same bases.

Val12 buries its methyl protons in the major groove near the H5 and H6 protons of C8 and U9 (not shown). Two key Arg residues facing the RNA from the same face of the β hairpin make specific contacts to the major groove faces of guanine bases: Arg1 contacts G9 (Figure 5B), and Arg3 contacts G11 (Figure 5C). Because Arg1 and Arg3 guanidinium NH_2 protons were not observed, the specific hydrogen-bonding mode for these Arg/guanine contacts cannot be unambiguously determined (parts B and C of Figure 5). However, the NOE contacts observed for the Hϵ proton of Arg1 and G9 are more consistent with the hydrogen bonds depicted in Figure 5B with the Arg1 Hϵ hydrogen bonded to N7 and HH21 hydrogen bonded to O6, rather than hydrogen bonds to the N7 and O6 involving exclusively the NH_2's, as often observed in protein−nucleic acid complexes (*60*). The aliphatic portion of the side chain of Arg5 stretches over U10 and makes a hydrophobic contact with the surface of that residue, completely caging and enclosing it along with I10 (parts D and E of Figure 5). The guanidinium group of Arg5 points directly at the space between G14 and C15, interacting with the nearby U12 phosphate while providing a cation−π interaction as well (Figure 5D). Arg8 contacts the tetraloop at the top of the structure stacking directly over A21 and may also contribute binding energy via a cation−π interaction with this base. The guanidinium group of Arg9 reaches back to interact with the phosphate between U20 and A21 and likely forms a salt bridge with it (Figure 5F). This contact is highly unexpected, because Arg9 is on the face of the β hairpin opposite to that where most of the residues important for the binding interaction are located. Arg11, on the peptide face opposite the RNA-binding surface, has only very limited contacts with the RNA but could assist in binding via electrostatic interactions with the nearby G22 phosphate. The remaining peptide residues (Val2 and Thr4 on the peptide face opposite the RNA, Gly6, and Lys7 in the type-II β turn and the D-Pro-L-Pro template) have no significant contacts to the BIV TAR RNA.

DISCUSSION

Treatment of HIV-infected patients is increasingly compromised by the development of resistance to existing drugs (*61*, *62*). New drugs are needed with orthogonal mechanisms of action compared to current drug targets. An attractive but unexploited target is the transactivator response element, TAR RNA, and its cognate transactivator protein Tat. Small molecules that disrupt the Tat/TAR interaction very likely will reduce HIV-1 replication rates by interfering with the transcription of viral genes. In the past, several TAR-binding small molecules (*2*, *3*, *27*−*29*, *32*, *34*, *37*) and peptide analogues (*20*, *22*, *23*, *25*) have been identified. However, these small molecules generally had poor activity and specificity (*27*, *29*). Peptide analogues had in at least one case some antiviral activity in cell-based assays (*20*) but were unstructured and had poor cell-penetration properties and stability. It proved impossible to develop clear structure−activity relationships or obtain critical structural information that would have allowed improvements in activity and selectivity of these initial leads. We reasoned that, as was the case for protein−protein complexes (*39*, *40*), it might be easier to inhibit these large intermolecular interfaces with

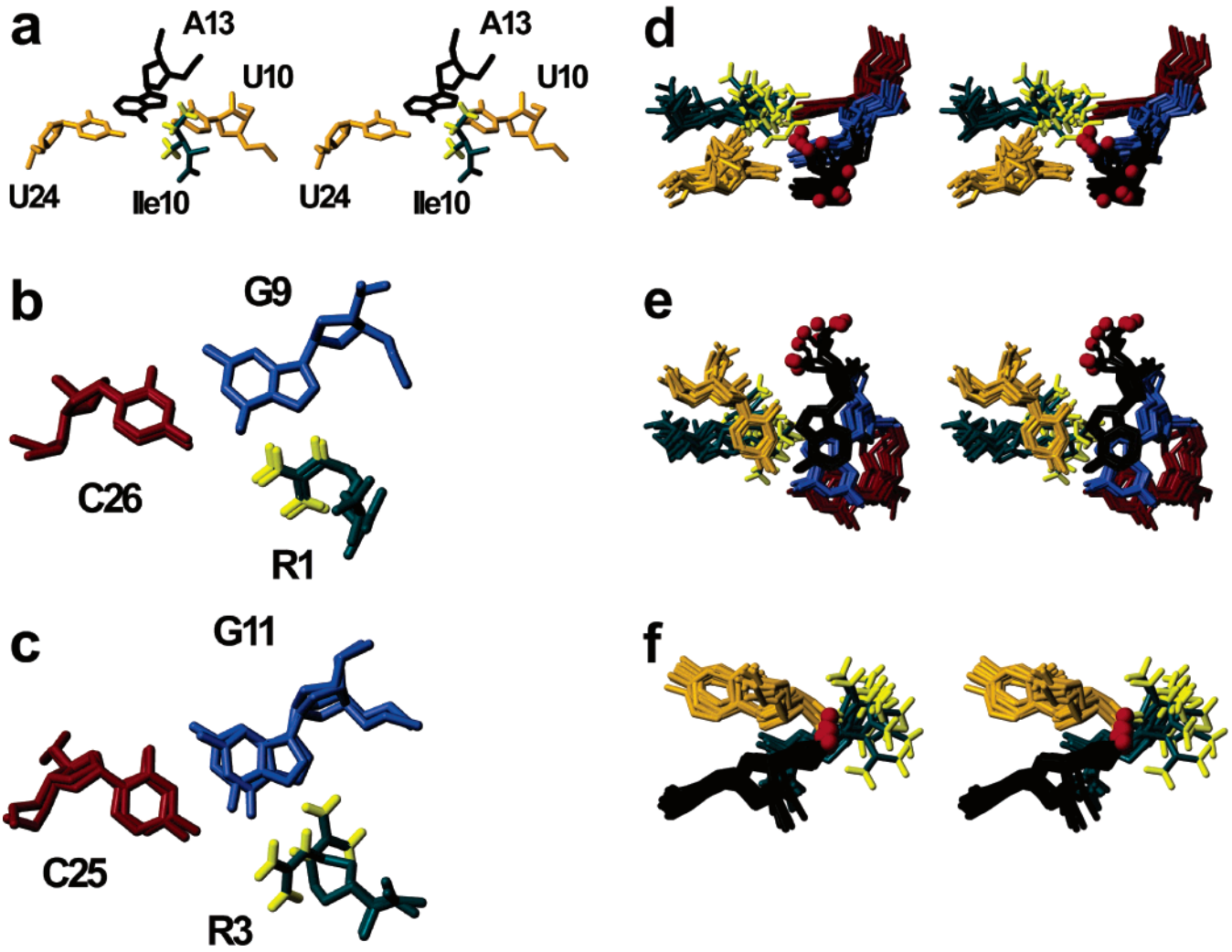

FIGURE 5: (a) Stereoview of the base-triple RNA residues around U10 contacted by Ile10 (green); methyl and methylene protons of Ile10 are rendered in yellow. (b and c) Arg1 and Arg3 (green) contacts to G−C pairs within the major groove; two representative structures from the 10-member ensemble are shown, indicating the degree of variability in the orientation of the guanidinium groups with respect to the N7 and O6 atoms of G9 (b) and G11 (c). Guanidinium NH_2 and Hϵ protons are rendered in yellow. (d) Stereoimages of the region of the structure surrounding Arg5, highlighting the cation−π interaction with U10; the A13 phosphate (red spheres) forms an electrostatic interaction with the same arginine. The position of the Arg5 guanidinium group is consistent with electrostatic interactions (nondirectional) rather than hydrogen bonds to G12. (e) Same as in d but rotated to show stacking of the Arg5 guanidinium group over U10. (f) Stereoview of the electrostatic interaction between the guanidinium group of Arg9 (green and yellow) and the phosphate of A21 (red).

conformationally constrained peptides as opposed to typical small "drug-like" molecules (*26*). We hypothesized that constrained peptides might provide more attractive peptidomimetic inhibitors of Tat proteins, as well as leads for the development of novel antiviral drugs.

Obviously, our target is the HIV Tat−TAR interaction, but there is no detailed structural information on the complex yet to allow for reliable peptidomimetic design. The structure of the BIV TAR RNA bound to a fragment of BIV Tat protein provided an alternative starting point (*17*, *26*, *42*). We reasoned that the close similarities in structure and sequence between HIV and BIV Tat and TAR elements would allow us to use the BIV model to identify initial leads for HIV Tat−TAR as well. This hypothesis has been validated by our recent discovery of specific inhibitors of the HIV Tat−TAR interaction among the family of peptidometics characterized in the present project (Athanassou et al., data not shown). We designed β-hairpin peptidomimetics by grafting the sequence of the RNA recognition element of BIV Tat onto the hairpin-inducing D-Pro-L-Pro template (*26*) but with several modifications (parts b and c of Figure 1). Gly76 in the wild-type peptide was removed to maintain an even number of amino acids on each strand, thereby favoring the formation of a cyclic β-hairpin structure. This deletion was expected to switch the β-turn conformation from type I to type II, because Lys75 and Gly76 that formed the turn in the Tat peptide were substituted with Gly6 and Lys7 (analogous to Gly74 and Lys75) in our library. Amino acids between Thr4 and Ile10 (analogous to Thr74 to Ile79 in the Tat-derived peptide) were kept the same as found in the BIV Tat protein. However, positions 1−3, 11, and 12 (analogous to positions 68−70, 80, and 81 in Tat) were varied during the library synthesis to search for variants that would stabilize the β-hairpin structure. When a very small eight-member peptide library was screened, we demonstrated a strong correlation between formation of the β-hairpin mimetic structure and the ability to bind to BIV TAR RNA tightly. The best inhibitor, BIV-2, bound to BIV TAR RNA with affinity comparable to the BIV Tat protein ($K_d \sim 150$ nM) (*26*). To probe how the peptide binds RNA and guides

further synthetic optimization of this compound, we determined the structure of the peptidomimetic−RNA complex by NMR.

BIV Tat−TAR is a classical example of recognition by induced fit, with the peptide becoming structured and the RNA changing conformation significantly upon binding (*63*). BIV-2 was designed to mimic Tat protein, which forms a β-hairpin structure only when bound to TAR. BIV-2 was shown to form a stable β-hairpin structure in aqueous solution (*26*). BIV-2 induces a conformational change in TAR, leading to a structure very similar to that of Tat-bound TAR RNA. Although BIV-2 binds to BIV TAR in an orientation that is flipped upside down compared to BIV Tat (Figure 4C), it retains key intermolecular contacts that direct the RNA conformational change. The Arg1, Arg3, Arg5, Ile10, and Val12 side chains were found to make the most extensive interactions with TAR. The side chains of these residues are all located on the upper face of the β hairpin, which provides a pre-organized scaffold to direct molecular recognition. Ile10, positioned in the middle of BIV-2, stabilizes the base triple by interacting with A13 and U24, as observed for Ile79 in the BIV Tat protein complex (Figure 5a). Arg5 was found to stack over U10 and to interact with G14 probably by forming a cation$-\pi$ interaction (parts d and e of Figure 5). Arg1 and Arg3 hydrogen bond to G9 and G11, and Val12 makes clear contacts to the H5/H6 faces of two pyrimidines, U7 and C8, and contributes to binding through these interactions. It was most fortuitous that this combination of residues, in positions 1−3, 11, and 12, were incorporated into one member of the small library of mimetics from which BIV-2 was isolated (*26*).

In the previous paper, we reported that the BIV-2 TAR interaction is specific in the sense that formation of a β hairpin is required for binding and even single amino acid substitutions caused relatively large changes in affinity (*26*). The structure of the complex illustrates how specificity in the BIV-2 TAR interaction is achieved by constraining the peptide and by positioning key functional groups at the interface with TAR RNA. Prestructuring the peptide reduces entropic costs upon binding and provides two key hydrophobic (Ile10 and Val12) interactions. Furthermore, hydrogen-bonding groups in Arg1 and Arg3 and the cation$-\pi$ interactions formed by Arg5 and Arg8 are achieved by the correct localization of these side chains relative to the RNA in its bound form. This way, the BIV-2 peptide already binds with affinity comparable to the RNA-binding domain of the Tat protein, although side-chain contacts remain to be further optimized.

The structure of BIV-2−TAR RNA complex clearly identifies positions that could tolerate structural changes without the substantial loss of binding affinity. First of all, all residues important for binding are on the upper surface of the peptide, while the side chains located in the lower face of the peptide are not significantly involved in TAR recognition. Guanidinium groups are required at positions 1, 3, and 5, while positions 10 and 12 should be occupied by hydrophobic residues. Thus, positions 1, 3, and 5 could be used to design functionality, i.e., cationic hydrogen-bonding donors, around the guanidinium group to increase affinity, while a variety of hydrophobic functionalities could be introduced at positions 10 and 12 to optimize intermolecular contacts. In contrast, Arg residues at positions 9 and 11 (important for BIV Tat binding to TAR) are not involved in BIV-2 binding to TAR and could be substituted to reduce the overall charge of the peptidomimetic. The partitioning of recognition characteristics could also be exploited to improve the pharmaceutical potential of this compound. The introduction of aliphatic and hydrophobic residues at positions 2, 4, 9, and 11 (on the lower face of the peptide) could increase the bioavailability of the ligand and its ability to penetrate cellular membranes.

In ongoing work, a new generation of peptidomimetics has been designed on the basis of these structural data and will be tested to identify more potent variants of BIV-2. In addition to proving that peptidomimetic chemistry could provide highly selective and potent inhibitors of key viral protein−RNA interactions, these second generation compounds will be used to search for inhibitors of the HIV Tat−TAR interaction based on the similarities between the two structures.

ACKNOWLEDGMENT

We acknowledge the financial support of NIH−NIAID and Dr. Oliver Zerbe (University of Zurich) for help in NMR data collection.

SUPPORTING INFORMATION AVAILABLE

BIV-2 peptide in complex with RNA at 298 K; BIV RNA in complex with BIV-2 at 298 and 275 K (iminos and aminos); BIV RNA free at 298 and 275 K (iminos and aminos); and BIV TAR shift changes upon BIV-2 binding. This material is available free of charge via the Internet at http://pubs.acs.org.

REFERENCES

1. Gait, M. J., and Karn, J. (1995) Progress in anti-HIV structure-based drug design, *Trends Biotechnol. 13*, 430−438.
2. Gallego, J., and Varani, G. (2001) Targeting RNA with small-molecule drugs: Therapeutic promise and chemical challenges, *Acc. Chem. Res. 34*, 836−843.
3. Sucheck, S. J., and Wong, C.-H. (2000) RNA as a target for small molecules, *Curr. Opin. Chem. Biol. 4*, 678−686.
4. Gait, M. J., and Karn, J. (1993) RNA recognition by the human immunodeficiency virus Tat protein and Rev protein, *Trends Biochem. Sci. 18*, 255−259.
5. Garber, M. E., Wei, P., KewalRamani, V. N., Mayall, T. P., Herrmann, C. H., Rice, A. P., Littman, D. R., and Jones, K. A. (1998) The interaction between HIV-1 Tat and human cyclin T1 requires zinc and a critical cysteine residue that is not conserved in the murine CycT1 protein, *Genes Dev. 12*, 3512−3527.
6. Wei, P., Garber, M. E., Fang, S.-M., Fischer, W. H., and Jones, K. A. (1998) A novel CDK9-associated C-type cyclin interacts directly with HIV-1 Tat and mediates its high-affinity, loop-specific binding to TAR RNA, *Cell 92*, 451−462.
7. Bieniasz, P. D., Grdina, T. A., Bogerd, H. P., and Cullen, B. R. (1998) Recruitment of a protein complex containing Tat and cyclin T1 to TAR governs the species specificity of HIV-1 Tat, *EMBO J. 17*, 7056−7065.
8. Fujinaga, K., Taube, R., Wimmer, J., Cujec, T. P., and Peterlin, B. M. (1999) Interactions between human cyclin T, Tat, and the transactivation response element (TAR) are disrupted by a cysteine to tyrosine substitution found in mouse cyclin T, *Proc. Natl. Acad. Sci. U.S.A. 96*, 1285−1290.
9. Richter, S., Ping, Y. H., and Rana, T. M. (2002) TAR RNA loop: A scaffold for the assembly of a regulatory switch in HIV replication, *Proc. Natl. Acad. Sci. U.S.A. 99*, 7928−7933.
10. Aboul-Ela, F., Karn, J., and Varani, G. (1995) The structure of the human immunodeficiency virus type-1 TAR RNA reveals

principles of RNA recognition by Tat protein, *J. Mol. Biol. 253*, 313−332.
11. Aboul-Ela, G., Karn, J., and Varani, G. (1996) Structure of HIV-1 TAR RNA in the absence of ligands reveals a novel conformation of the trinucleotide bulge, *Nucleic Acids Res. 24*, 4598−4598.
12. Brodsky, A. S., and Williamson, J. R. (1997) Solution structure of the HIV-2 TAR−argininamide complex, *J. Mol. Biol. 267*, 624−639.
13. Brodsky, A. S., Erlacher, H. A., and Williamson, J. R. (1998) NMR evidence for a base triple in the HIV-2 TAR C−G•C+ mutant argininamide complex, *Nucleic Acids Res. 26*, 1991−1995.
14. Long, K. S., and Crothers, D. M. (1999) Characterization of the solution conformations of unbound and Tat peptide-bound forms of HIV-1 TAR RNA, *Biochemistry 38*, 10059−10069.
15. Du, Z. H., Lind, K. E., and James, T. L. (2002) Structure of TAR RNA complexed with a Tat−TAR interaction nanomolar inhibitor that was identified by computational screening, *Chem. Biol. 9*, 707−712.
16. Greenbaum, N. L. (1996) How Tat targets TAR: Structure of the BIV peptide RNA complex, *Structure 4*, 5−9.
17. Puglisi, J. D., Chen, L., Blanchard, S., and Frankel, A. D. (1995) Solution structure of a bovine immunodeficiency virus Tat−TAR peptide−RNA Complex, *Science 270*, 1200−1203.
18. Puglisi, J. D., Chen, L., Frankel, A. D., and Williamson, J. R. (1993) Role of RNA structure in arginine recognition of TAR RNA, *Proc. Natl. Acad. Sci. U.S.A. 90*, 3680−3684.
19. Ippolito, J. A., and Steitz, T. A. (1998) A 1.3 Å resolution crystal structure of the HIV-1 trans-activation response region RNA stem reveals a metal ion-dependent bulge conformation, *Proc. Natl. Acad. Sci. U.S.A. 95*, 9819−9824.
20. Hamy, F., Felder, E. R., Heizmann, G., Lazdins, J., Aboul-Ela, F., Varani, G., Karn, J., and Klimkait, T. (1997) An inhibitor of the Tat/TAR RNA interaction that effectively suppresses HIV-1 replication, *Proc. Natl. Acad. Sci. U.S.A. 94*, 3548−3553.
21. Huq, I., Wang, X. L., and Rana, T. M. (1997) Specific recognition of HIV-1 TAR RNA by a D-Tat peptide, *Nat. Struct. Biol. 4*, 881−882.
22. Hwang, S., Tamilarasu, N., Ryan, K., Huq, I., Richter, S., Still, W. C., and Rana, T. M. (1999) Inhibition of gene expression in human cells through small molecule−RNA interactions, *Proc. Natl. Acad. Sci. U.S.A. 96*, 12997−13002.
23. Tamilarasu, N., Huq, I., and Rana, T. M. (2001) Targeting RNA with peptidomimetic oligomers in human cells, *Bioorg. Med. Chem. Lett. 11*, 505−507.
24. Wang, X. L., Huq, I., and Rana, T. M. (1997) HIV-1 TAR RNA recognition by an unnatural biopolymer, *J. Am. Chem. Soc. 119*, 6444−6445.
25. Runyon, S. T., and Puglisi, J. D. (2003) Design of a cyclic peptide that targets a viral RNA, *J. Am. Chem. Soc. 125*, 15704−15705.
26. Athanassiou, Z., Dias, R. L. A., Moehle, K., Dobson, N., Varani, G., and Robinson, J. A. (2004) Structural mimicry of retroviral Tat proteins by constrained, β-hairpin peptidomimetics: Ligands with high affinity and selectivity for viral TAR RNA regulatory elements, *J. Am. Chem. Soc. 126*, 6906−6913.
27. Davis, B., Afshar, M., Varani, G., Murchie, A. I. H., Karn, J., Lentzen, G., Drysdale, M., Bower, J., Potter, A. J., Starkey, I. D., Swarbrick, T., and Aboul-Ela, F. (2004) Rational design of inhibitors of HIV-1 TAR RNA through the stabilisation of electrostatic "hot spots", *J. Mol. Biol. 336*, 343−356.
28. Lee, J. K., Kwon, M. Y., Lee, K. H., Jeong, S. J., Hyun, S., Shin, K. J., and Yu, J. H. (2004) An approach to enhance specificity against RNA targets using heteroconjugates of aminoglycosides and chloramphenicol (or linezolid), *J. Am. Chem. Soc. 126*, 1956−1957.
29. Murchie, A. I. H., Davis, B., Isel, C., Afshar, M., Drysdale, M. J., Bower, J., Potter, A. J., Starkey, I. D., Swarbrick, T. M., Mirza, S., Prescott, C. D., Vaglio, P., Aboul-Ela, F., and Karn, J. (2004) Structure-based drug design targeting an inactive RNA conformation: Exploiting the flexibility of HIV-1 TAR RNA, *J. Mol. Biol. 336*, 625−638.
30. Blount, K. F., and Tor, Y. (2003) Using pyrene-labeled HIV-1 TAR to measure RNA−small molecule binding, *Nucleic Acids Res. 31*, 5490−5500.
31. Hwang, S., Tamilarasu, N., Kibler, K., Cao, H., Ali, A., Ping, Y. H., Jeang, K. T., and Rana, T. M. (2003) Discovery of a small molecule Tat-trans-activation-responsive RNA antagonist that potently inhibits human immunodeficiency virus-1 replication, *J. Biol. Chem. 278*, 39092−39103.
32. Lind, K. E., Du, Z. H., Fujinaga, K., Peterlin, B. M., and James, T. L. (2002) Structure-based computational database screening, *in vitro* assay, and NMR assessment of compounds that target TAR RNA, *Chem. Biol. 9*, 185−193.
33. Faber, C., Sticht, H., Schweimer, K., and Rosch, P. (2000) Structural rearrangements of HIV-1 Tat-responsive RNA upon binding of neomycin B, *J. Biol. Chem. 275*, 20660−20666.
34. Hamy, F., Gelus, N., Zeller, M., Lazdins, J. L., Bailly, C., and Klimkait, T. (2000) Blocking HIV replication by targeting Tat protein, *Chem. Biol. 7*, 669−676.
35. Ecker, D. J., and Griffey, R. H. (1999) RNA as a small-molecule drug target: Doubling the value of genomics, *Drug Discovery Today 4*, 420−429.
36. Gelus, N., Bailly, C., Hamy, F., Klimkait, T., Wilson, W. D., and Boykin, D. W. (1999) Inhibition of HIV-1 Tat−TAR interaction by diphenylfuran derivatives: Effects of the terminal basic side chains, *Bioorg. Med. Chem. 7*, 1089−1096.
37. Hamy, F., Brondani, V., Florsheimer, A., Stark, W., Blommers, M. J. J., and Klimkait, T. (1998) A new class of HIV-1 Tat antagonist acting through Tat−TAR inhibition, *Biochemistry 37*, 5086−5095.
38. Wang, S. H., Huber, P. W., Cui, M., Czarnik, A. W., and Mei, H. Y. (1998) Binding of neomycin to the TAR element of HIV-1 RNA induces dissociation of Tat protein by an allosteric mechanism, *Biochemistry 37*, 5549−5557.
39. Gadek, T. R., Burdick, D. J., McDowell, R. S., Stanley, M. S., Marsters, J. C., Paris, K. J., Oare, D. A., Reynolds, M. E., Ladner, C., Zioncheck, K. A., Lee, W. P., Gribling, P., Dennis, M. S., Skelton, N. J., Tumas, D. B., Clark, K. R., Keating, S. M., Beresini, M. H., Tilley, J. W., Presta, L. G., and Bodary, S. C. (2002) Generation of an LFA-1 antagonist by the transfer of the ICAM-1 immunoregulatory epitope to a small molecule, *Science 295*, 1086−1089.
40. Gadek, T. R., and McDowell, R. S. (2003) Discovery of small molecule leads in a biotechnology datastream, *Drug Discovery Today 8*, 545−550.
41. Chen, L., and Frankel, A. D. (1994) An RNA-binding peptide from bovine immunodeficiency virus Tat protein recognizes an unusual RNA structure, *Biochemistry 33*, 2708−2715.
42. Ye, X. M., Kumar, R. A., and Patel, D. J. (1995) Molecular recognition in the bovine immunodeficiency virus Tat peptide TAR RNA complex, *Chem. Biol. 2*, 827−840.
43. Price, S. R., Oubridge, C., Varani, G., and Nagai, K. (1998) in *RNA−Protein Interaction: Practical Approach* (Smith, C., Ed.) pp 37−74, Oxford University Press, New York.
44. Delaglio, F., Grzesiek, S., Vuister, G. W., Zhu, G., Pfeifer, J., and Bax, A. (1995) nmrPipe—A multidimensional spectral processing system based on unix pipes, *J. Biomol. NMR 6*, 277−293.
45. Goddard, T. D., and Kneller, D. G. *Sparky 3*, University of California, San Francisco, CA.
46. Varani, G., Aboul-Ela, F., Allain, F., and Gubser, C. C. (1995) Novel 3-dimensional H^1, C^{13}, P^{31} triple-resonance experiments for sequential backbone correlations in nucleic acids, *J. Biomol. NMR 5*, 315−320.
47. Heus, H. A., Wijmenga, S. S., Vandeven, F. J. M., and Hilbers, C. W. (1994) Sequential backbone assignment in C-13-labeled RNA via through-bond coherence transfer using 3-dimensional triple-resonance spectroscopy (H^1, C^{13}, P^{31}) and 2-dimensional hetero TOCSY, *J. Am. Chem. Soc. 116*, 4983−4984.
48. Peterson, R. D., Theimer, C. A., Wu, H. H., and Feigon, J. (2004) New applications of 2D filtered/edited NOESY for assignment and structure elucidation of RNA and RNA−protein complexes, *J. Biomol. NMR 28*, 59−67.
49. Zwahlen, C., Legault, P., Vincent, S. J. F., Greenblatt, J., Konrat, R., and Kay, L. E. (1997) Methods for measurement of intermolecular NOEs by multinuclear NMR spectroscopy: Application to a bacteriophage λ N-peptide/boxB RNA complex, *J. Am. Chem. Soc. 119*, 6711−6721.
50. Shaka, A. J., Lee, C. J., and Pines, A. (1988) Iterative schemes for bilinear operators—Application to spin decoupling, *J. Magn. Reson. 77*, 274−293.
51. Varani, G., Aboul-Ela, F., and Allain, F. H. T. (1996) NMR investigation of RNA structure, *Prog. Nucl. Mag. Reson. Spectrosc. 29*, 51−127.
52. Pardi, A., and Nikonowicz, E. P. (1992) Simple procedure for resonance assignment of the sugar protons in C-13-labeled RNAs, *J. Am. Chem. Soc. 114*, 9202−9203.

53. Hansen, M. R., Mueller, L., and Pardi, A. (1998) Tunable alignment of macromolecules by filamentous phage yields dipolar coupling interactions, *Nat. Struct. Biol. 5*, 1065−1074.
54. Andersson, P., Nordstrand, K., Sunnerhagen, M., Liepinsh, E., Turovskis, I., and Otting, G. (1998) Heteronuclear correlation experiments for the determination of one-bond coupling constants, *J. Biomol. NMR 11*, 445−450.
55. Schwieters, C. D., Kuszewski, J. J., Tjandra, N., and Clore, G. M. (2003) The Xplor-NIH NMR molecular structure determination package, *J. Magn. Reson. 160*, 65−73.
56. Brunger, A. T., Adams, P. D., Clore, G. M., DeLano, W. L., Gros, P., Grosse-Kunstleve, R. W., Jiang, J. S., Kuszewski, J., Nilges, M., Pannu, N. S., Read, R. J., Rice, L. M., Simonson, T., and Warren, G. L. (1998) Crystallography and NMR system: A new software suite for macromolecular structure determination, *Acta Crystallogr., Sect. D: Biol. Crystallogr. 54*, 905−921.
57. Al-Hashimi, H. M., Gosser, Y., Gorin, A., Hu, W. D., Majumdar, A., and Patel, D. J. (2002) Concerted motions in HIV-1 TAR RNA may allow access to bound state conformations: RNA dynamics from NMR residual dipolar couplings, *J. Mol. Biol. 315*, 95−102.
58. Leeper, T. C., and Varani, G. (2005) The structure of an enzyme-activating fragment of human telomerase RNA, *RNA 11*, 394−403.
59. Koradi, R., Billeter, M., and Wuthrich, K. (1996) MOLMOL: A program for display and analysis of macromolecular structures, *J. Mol. Graphics 14*, 51.
60. Chen, Y., Kortemme, T., Robertson, T., Baker, D., and Varani, G. (2004) A new hydrogen-bonding potential for the design of protein−RNA interactions predicts specific contacts and discriminates decoys, *Nucleic Acids Res. 32*, 5147−5162.
61. Larder, B. A., and Stammers, D. K. (1999) Closing in on HIV drug resistance, *Nat. Struct. Biol. 6*, 103−106.
62. Perrin, L., and Telenti, A. (1998) HIV treatment failure: Testing for HIV resistance in clinical practice, *Science 280*, 1871−1873.
63. Leulliot, N., and Varani, G. (2001) Current topics in RNA−protein recognition: Control of specificity and biological function through induced fit and conformational capture, *Biochemistry 40*, 7947−7956.

BI0510532